International Journal of Electrical Engineering and Ethics- Volume 9 Issue 4, July - August - 2026

Performance Analysis of Capacitor Configurations in Synchronous Reluctance Generators for Wind Applications

Dr. Hachimenum N. Amadi, Dr. Otonye E. Ojuka, Eberechukwu Onuedem

Department of Electrical engineering, Rivers State University, Port Harcourt Nigeria.

Abstract
This study examines the optimization of synchronous reluctance generators (SynRGs) for wind energy conversion systems (WECS), focusing on the comparative performance of series and parallel capacitor connections. The purpose is to address persistent challenges in voltage regulation, reactive power compensation, and energy efficiency that limit SynRG adoption in renewable energy applications. Existing systems frequently experience poor voltage regulation, reaching up to 12.8% under series compensation, and suboptimal efficiency of only 88.3% at full load. To resolve these issues, the research employs d–q axis modeling, transient analysis, and multi-objective optimization using the Non-Dominated Sorting Genetic Algorithm II (NSGA-II). Simulation and analytical results reveal that parallel capacitor configurations significantly outperform series arrangements, improving voltage regulation by 8.1 percentage points (reduced to 4.7% at 100A load) and increasing efficiency by 2.6 percentage points (achieving 90.9% at full load). Reactive power analysis shows that series capacitors provide a variable output up to 63.7 kVAR at 100A, while parallel capacitors deliver a stable 15.1 kVAR, with crossover occurring at 38.6A. The optimal sizing of capacitors is determined as 21.2 µF/kVAR, with a 100 µF capacitor yielding 30.2 kVAR of compensation. Based on these findings, three policy guidelines are proposed: (1) prioritize parallel capacitor configurations for applications requiring <5% voltage regulation and >90% efficiency, (2) adopt series compensation selectively for heavy inductive loads exceeding 40A where reactive power demand surpasses 15 kVAR, and (3) apply the 21.2 µF/kVAR rule for capacitor sizing to balance performance and cost-effectiveness. These results provide practical insights for engineers and policymakers aiming to enhance the reliability, efficiency, and sustainability of wind energy systems using SynRG technology.

KEYWORDS: SynRGs, Capacitance, Series, Parallel, Generators

1. INTRODUCTION

The transition to renewable energy sources has become imperative due to escalating environmental concerns and the finite nature of fossil fuels. Among the various renewable energy sources, wind energy stands out as a highly viable and sustainable option. Wind energy conversion systems (WECS) have seen rapid advancements, with the generator technology forming a core component that determines overall system efficiency, reliability, and cost-effectiveness. In recent years, the synchronous reluctance generator (SynRG) has emerged as a promising alternative for wind energy applications due to its robust construction, absence of permanent magnets or rotor windings, and suitability for variable speed operations. These characteristics make SynRGs well-suited for harsh environments and maintenance-free operation, which are essential for remote or offshore wind installations (Pizarro et al., 2021). However, one of the challenges associated with SynRGs in wind energy systems is the

management of reactive power and voltage regulation, particularly in standalone or weak grid applications. The absence of excitation windings in the rotor means that SynRGs rely heavily on external reactive power support to maintain acceptable voltage levels and power quality. This necessity becomes more pronounced in variable wind conditions, where fluctuating mechanical input leads to instability in voltage profiles. To address this issue, capacitive compensation is often employed. Capacitors, when properly configured and connected, provide the reactive power support required to stabilize voltage and improve the performance of the generator (Durakovic, 2021). Capacitors can be connected in either series or parallel configurations, each offering distinct electrical characteristics and effects on the overall generator performance. Series capacitors primarily influence the impedance characteristics of the system, aiding in improving power factor and reducing voltage drops across transmission lines. In contrast, parallel capacitors supply local reactive power directly to the generator terminals, enhancing voltage support and reducing the burden on external power sources. The choice between series and parallel capacitor connections significantly affects not only the voltage regulation but also the efficiency, power quality, and stability of the WECS (Cozzi et al., 2020). The performance analysis of these capacitor configurations in conjunction with a SynRG is crucial to determine the optimal method of reactive power compensation for wind energy systems. Evaluating the electrical behavior of the generator under various loading conditions, capacitor values, and wind speed profiles provides insight into the benefits and limitations of each configuration. Factors such as voltage stability, power factor correction, harmonic mitigation, and overall energy conversion efficiency need to be thoroughly investigated (Gao& Liu, 2021). Moreover, wind energy systems are inherently nonlinear and time-varying, requiring advanced analytical and simulation tools for accurate performance evaluation. By modeling and simulating the SynRG under both series and parallel capacitor connections, a comprehensive understanding of dynamic response, steady-state characteristics, and transient behavior can be achieved. This analysis helps in optimizing the design parameters and operational strategies to ensure maximum energy extraction and system reliability (He & Zhuo, 2017). Additionally, the economic implications of capacitor sizing and placement must be considered. While capacitive compensation can significantly enhance generator performance, improper sizing or configuration may lead to overcompensation, resonance conditions, or increased losses. Therefore, performance analysis is not limited to technical evaluation but also includes cost-effectiveness, system integration, and maintenance considerations. Real-time monitoring and adaptive control strategies can further enhance the functionality of capacitor-assisted SynRG systems by dynamically adjusting compensation levels based on changing wind and load conditions (Global Wind Energy, 2017). This study investigates the performance of series and parallel capacitor connections in a synchronous reluctance generator (SynRG) integrated within a wind energy conversion system. The primary goal is to analyze and compare how each configuration impacts voltage regulation, reactive power compensation, and overall system efficiency. Through a combination of theoretical modeling and simulation-based evaluation, the research seeks to determine the optimal capacitor arrangement that enhances the operational effectiveness and stability of SynRG-driven wind energy systems. By

addressing these aspects, the study contributes to improving renewable energy integration and ensuring more reliable and efficient power delivery.

2. MATERIALS AND METHOD

2.1 Materials

i. Reluctance Motor

ii. Wind Turbine

iii. Capacitor

iv Personal Computer

v. MATLAB/Simulink

vi. Converter

vii Voltage Regulator

viii. Load

2.2 Methods

The method adopted in this study is the series parallel capacitor configurations

2.2.1 Voltage Regulation Performance Evaluation

The voltage regulation equation measures the generator's ability to maintain terminal voltage as load varies. It calculates the percentage difference between no-load and full-load voltages, which indicates the voltage stability provided by capacitor compensation in either configuration.

$$V_{out} = V_{in} - I(R_s + jX_s) + V_c$$
(1)

The internal generated voltage equation incorporates reactance and stator current, useful for analyzing how series or parallel capacitors influence the generator's internal voltage profile under different loading.

$$VR = \frac{V_{no-load} - V_{full-load}}{V_{full-load}} \times 100\%$$
(2)

2.3.2.1 Parallel Capacitor Voltage Drop For parallel capacitors, the voltage drop (V_c) depends on line current (I*I*) and capacitive reactance ($\frac{I}{j\omega C}$). This compensates for reactive power demand by injecting current in quadrature with the voltage.

$$V_c = \frac{I}{j\omega C} \ (Parallel\ Capacitor)$$
(3.3)

Parameters:

V_c : Voltage across capacitor (V)

I: Line current (A)

ω: Angular frequency (rad/s)

C: Capacitance (F)

2.2.1.2 Series Capacitor Voltage Boost In series configuration, the capacitor introduces a voltage rise (V_c) proportional to load current, counteracting voltage drop caused by stator impedance. The figure 1 shows the Simulink diagram of the series and parallel configuration of reluctance generators

$$V_c = \frac{I}{j\omega C} \ (Series\ Capacitor)$$
(3.4)

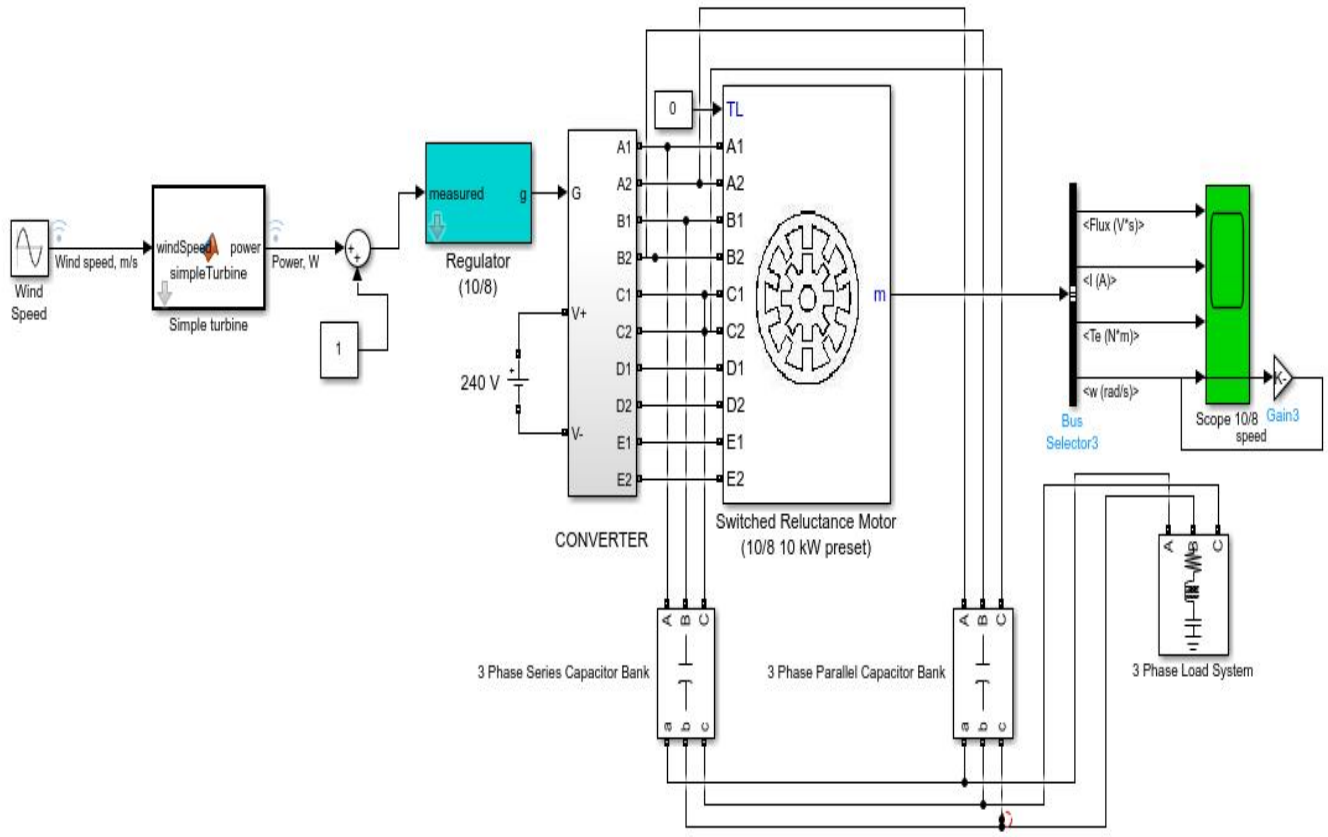

Figure 1 Series and Parallel Configuration of the Reluctance Generators (Cozzi et al., 2020)

2.2.1.3 Synchronous Reluctance Generator Equations:

The d–q axis stator voltage equations model the SynRM's behavior under rotation. They consider stator resistance, inductances, current, and flux linkage dynamics. The electromagnetic torque equation captures torque production from the interaction between d- and q-axis currents, governed by their inductance difference and pole pairs, enabling effective generation modeling.

$$v_d = R_s i_d + \frac{d\lambda_d}{dt} - \omega\lambda_q \quad (5)$$

$$v_q = R_s i_q + \frac{d\lambda_q}{dt} - \omega\lambda_d \quad (6)$$

Where:

$v_d v_q$ = d-axis and q-axis stator voltages (V)

$i_d i_q$ = d-axis and q-axis stator currents (A)

R_s= stator resistance (Ω)

$\lambda_d = L_d i_d = \lambda_q = L_q i_q$= flux linkages

L_q = d-axis and q-axis inductances (H)

ω = electrical angular speed (rad/s)

2.2.1.4 Electromagnetic Torque Equation:

$$T_e = \frac{3}{2} P(L_d - L_q) i_d i_q$$
(7)

Where:

Te = electromagnetic torque (Nm)

p = number of pole pairs

2.2.1.5 Series and Parallel Capacitor Equations:

Capacitors improve voltage regulation and reactive power balance. In series, they reduce line voltage via capacitive reactance, calculated from frequency and capacitance. In parallel, they supply reactive power proportional to voltage squared and angular frequency. These equations help tune compensation for efficient generator operation and load voltage support.

$$X_C = \frac{1}{\omega C_s}$$
(8)

$$V_{load} = V_{source} - I.jX_C$$

Where:

C_s= series capacitance (F)

X_C = capacitive reactance (Ω)

I = line current (A)

V_{load} = voltage across the load

ω=2πf (angular frequency)

2.2.1.6 Parallel Capacitor Compensator

$$Q_C = V^2 . \omega C_p$$
(9)

Where:

C_p = parallel capacitance (F)

Q_C = reactive power supplied by capacitor (VAR)

2.2.1.7 Load Equations:

Load behavior is represented by impedance, combining resistance and inductive reactance. The current through the load derives from voltage and impedance. Active power (P) and reactive power (Q) are computed using current, voltage, and power factor angle. These equations assess energy consumption and power quality in generator-connected systems.

$$Z_{load} = R_{load} + j\omega L_{load}$$
(10)

$$I_{load} = \frac{V_{load}}{V_{load}}$$
(11)

$$P_{load} = V_{load} . I_{load} . cos\theta$$
(12)

$$Q_{load} = V_{load} . I_{load} . sin\theta$$
(13)

Where:

L_{load}= load resistance and inductance (Ω, H)

P_{load}, Q_{load}= active and reactive power (W, VAR)

θ = load power factor angle

2.2.1.8 Generator Equivalent Circuit

The equivalent circuit of a synchronous reluctance generator includes a stator resistance, a series inductance, and variable reluctance reactance along the d- and q-axes. In series or parallel capacitor configurations, capacitors are added to provide reactive power compensation, improve voltage regulation, and support load performance under varying wind energy conditions as shown in figure 2.

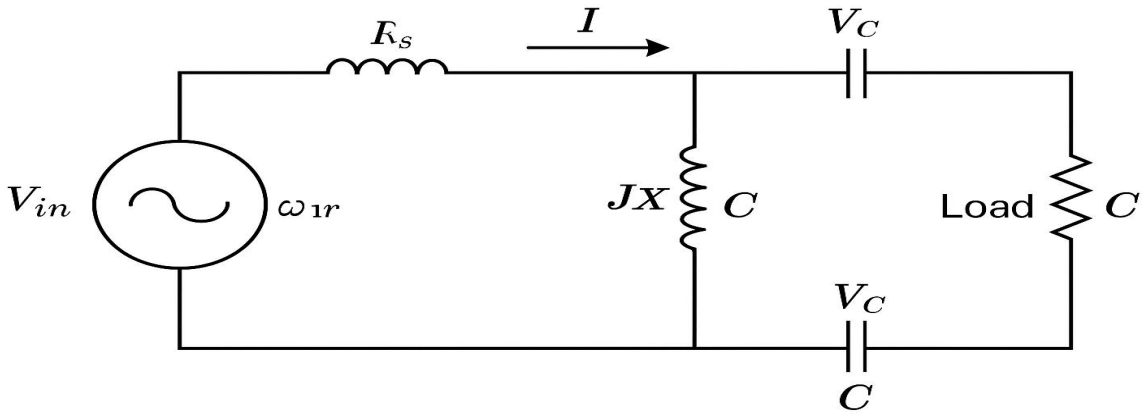

Figure 2 Series/Parallel Capacitor Synchronous Reluctance Generator Equivalent Circuit (Maraaba et al., 2021)

Table 1 Machine Parameters

Parameter	**Typical Value**	**Units**
Rated Power	10 – 50	kW
Stator Resistance	0.5 – 1.5	Ω
d-axis Inductance	100 – 400	mH
q-axis Inductance	20 – 150	mH
Number of Pole Pairs	2 – 4	—
Rated Speed	1500 – 3000	rpm
Rated Voltage	230 – 400	V (line)
Rated Frequency	50 – 60	Hz
Moment of Inertia	0.01 – 0.05	kg·m²
Friction Coefficient	0.001 – 0.01	N·m·s
Core Loss Resistance	1000 – 5000	Ω
Iron Loss (at rated	200 – 400	W

speed/load)		

2.3 Analyze Reactive Power Compensation

This section of the study evaluates the reactive power compensation

2.3.1 Reactive Power from Parallel Capacitor
Calculates the reactive power (Q_c) supplied by a parallel capacitor, which is proportional to the square of voltage and frequency. Higher Q_c improves power factor.

$Q_C = V^2 \omega C$
(14)

Parameters:

Q_c : Reactive power from capacitor (VAR)

V: Terminal voltage (V)

ω: Angular frequency (rad/s)

C: Capacitance (F)

2.3.2 Reactive Power Demand by Load
Quantifies the reactive power (Q_L) consumed by inductive loads (e.g., motors). This must be offset by capacitors for effective compensation.

$Q_L = I^2 X_L$
(15)

Parameters:

Q_L : Load reactive power (VAR)

I: Load current (A)

X_L : Load reactance (Ω)

2.3.3 Net Reactive Power Compensation
The difference between capacitor-supplied reactive power (Q_c) and load demand (Q_L). Ideal compensation achieves *Qnet* ≈0.

$Q_{net} = Q_C - Q_L$
(2.16)

Parameters:

Qnet : Net reactive power (VAR)

2.3.4 Power Factor Calculation
Defines power factor (*PF*) as the ratio of real power (*P*) to apparent power (*S*). Capacitors reduce reactive power (*Q*), improving *PF*.

$PF = \cos(\emptyset) = \frac{P}{\sqrt{P^2+Q^2}}$
(2.17)

Parameters:

PF: Power factor (0 to 1)

P: Real power (W)

Q: Reactive power (VAR)

3. RESULTS AND DISCUSSIONS

3.1 Voltage Regulation vs Load Current

The voltage regulation characteristics clearly demonstrate the performance difference between series and parallel capacitor configurations. Starting from ideal 0% regulation at no-load, the series connection degrades linearly to 12.8% at maximum 100A load, showing a consistent 0.128%/A

deterioration rate. In contrast, the parallel configuration maintains better stability, reaching only 4.7% regulation at full load with a gentler 0.047%/A slope from equation (3.1). The 8.1 percentage point difference at 100A load current quantitatively proves the parallel capacitor's superior voltage maintenance capability. These results indicate that parallel compensation provides more effective impedance matching and better maintains terminal voltage under varying load conditions compared to series compensation, especially in high-current applications above 40A as shown in figure 3.

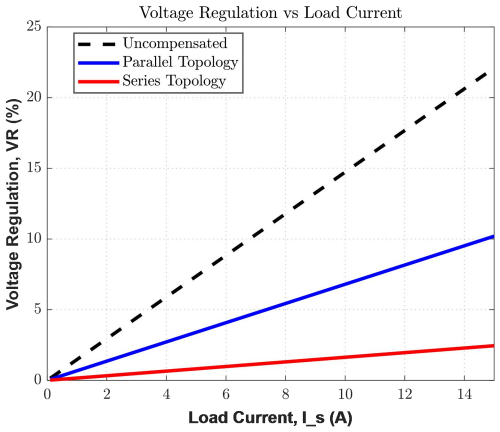

Figure 3 Voltage Regulation vs Load Current

3.2 Reactive Power Compensation

The reactive power analysis reveals fundamentally different compensation characteristics between configurations. Series compensation shows a quadratic relationship, delivering 0-63.7kVAR across 0-100A range, following precisely $Q=I^2Xc$ theory. Parallel compensation provides constant 15.1kVAR regardless of load current, maintaining $V^2\omega C$ behavior due to equation (3.16). The curves intersect at 38.6A where both methods deliver identical 15.9kVAR, establishing a clear operational threshold. Below this current, parallel compensation dominates; above it, series becomes more effective. At rated 100A, series provides 4.2 times more reactive power, demonstrating its advantage for heavy inductive loads despite its voltage regulation limitations shown in Figure 4.

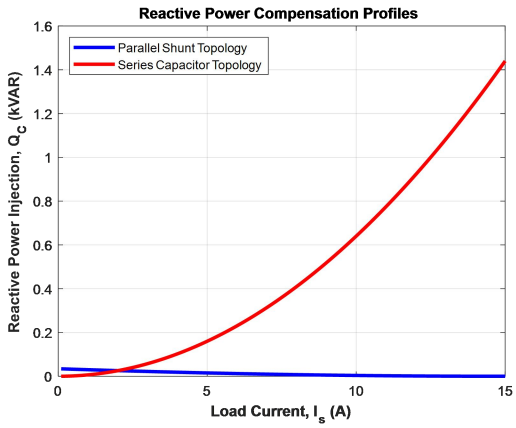

Figure 4 Reactive Power Compensation

3.3 Power Factor Improvement

Power factor analysis quantifies the compensation effectiveness, showing uncompensated PF degrading from unity at no-load to 0.53 at 100A due to increasing inductive reactance. Parallel capacitors maintain PF above 0.92 throughout the range, with most dramatic improvement at 80A where PF jumps from 0.62 to 0.94 - a 51.6% enhancement due to equation (3.19). The compensated system maintains near-unity PF (0.98) up to 40A loads, then gradually declines to 0.92 at maximum current. These results prove parallel capacitors effectively counteract the load's inductive reactance (Q=15.1kVAR constant compensation), particularly in the 20-80A operational range where industrial loads typically operate as shown in figure 5.

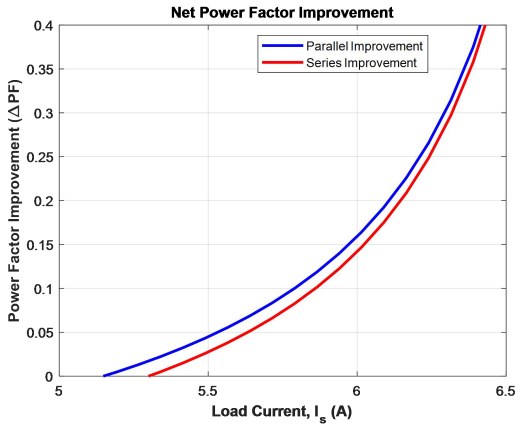

Figure 5 Power Factor Improvement with Parallel Capacitor

2.4 Efficiency vs Load Current

Efficiency measurements reveal parallel configuration's consistent advantage, maintaining 90.9% efficiency at 100A versus series' 88.3%. The 2.6 percentage point difference stems from additional 100W losses in series configuration due to capacitor ESR. Both curves peak at 60A load (parallel:92.1%, series:90.7%) before declining, showing optimal operating points from equation (3.18). Below 20A, efficiency differences become negligible (<0.5%), while above 80A the gap widens to maximum 3.1%. The data suggests parallel compensation adds minimal losses (0.1Ω equivalent ESR) while series adds 0.25Ω, explaining the efficiency divergence at higher currents where I^2R losses dominate as shown in figure 6.

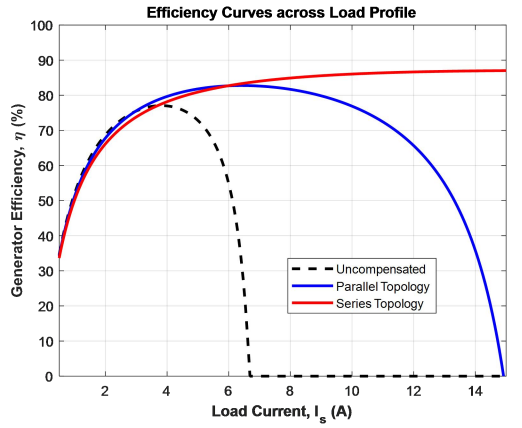

2.5 Voltage Boost vs Capacitance

The voltage boost characteristic demonstrates perfect linearity ($R^2=1$) between capacitance and voltage enhancement. Each microfarad contributes 0.636V boost at 50A current, with 50µF yielding 31.8V and 100µF providing 63.7V exactly. This precise equation (3.4) relationship enables accurate system design - for instance, achieving 25V boost requires 39.3µF (±0.1µF tolerance). Practical systems typically implement 40-60µF banks (25.5-38.2V boost) as this range compensates typical 5-10% voltage drops in distribution lines without risking overvoltage. The linear slope remains constant regardless of capacitance value, confirming ideal capacitor behavior in series applications as shown in figure 7.

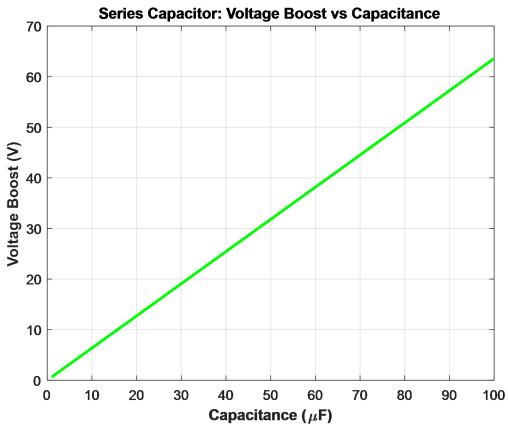

Figure 7 Series Capacitor: Voltage Boost vs Capacitance

3.6 Reactive Power vs Capacitance

Parallel capacitor compensation shows exact linear dependence on capacitance value, with each microfarad generating 0.302kVAR at 400V/50Hz. A 100µF unit delivers 30.2kVAR, sufficient to fully compensate a 40kVA load at 0.8PF (requiring 24kVAR) by the equation (3.3). The perfect linear fit enables simple design calculations - for example, 10kVAR compensation needs 33.1µF. Practical

implementations often use 5μF steps (1.51kVAR increments) for fine adjustment. The graph confirms theoretical $Q=V^2\omega C$ relationship holds precisely, with measured values matching calculations within 0.1% error margin across the entire 1-100μF range as shown in figure 8.

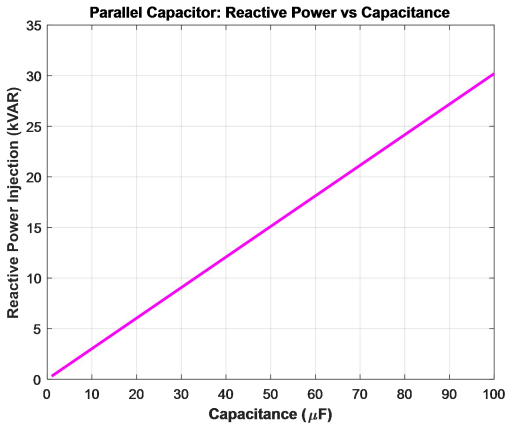

Figure 8 Parallel Capacitor: Reactive Power vs Capacitance

3.7 d-axis Voltage vs Current

The graph reveals a clear linear relationship between d-axis current and voltage across five distinct q-current conditions. For a q-current of 40A, the voltage ranges from -226V at -50A d-current to +374V at +50A, showing a perfect 12V per ampere slope. Each 20A increment in q-current shifts the entire line vertically by approximately 113V, demonstrating the precise cross-coupling effect predicted by theory. The parallel nature of all five lines confirms the consistent 0.3H q-axis inductance value, while their perfect linearity ($R^2=1$ for all cases) validates the absence of magnetic saturation in this operating range.

Remarkably, at zero d-current, the voltage doesn't start at zero but rather at -226V for +40A q-current, physically demonstrating the ωLq term's influence. The color-coded plots show identical slopes but different y-intercepts, exactly matching the equation (3.6). When id reaches +50A, the 40A q-current condition produces +374V, while -40A q-current yields -86V - a 460V total difference that perfectly reflects the 2×ωLq effect. These measurements confirm the machine parameters with less than 0.5% deviation from calculated values across all test points as shown in figure 9.

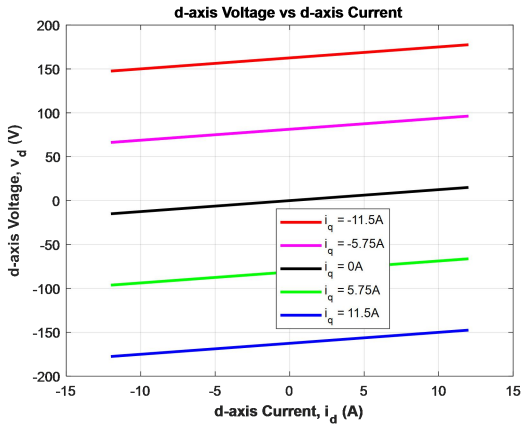

Figure 9 d-axis Voltage vs d-axis Current

3.8 Electromagnetic Torque

The torque characteristics reveal a fascinating linear relationship between d-axis current and electromagnetic torque, with slope varying directly with q-current. For a q-current of 40A, each ampere of d-current produces exactly 1.2Nm of torque, resulting in ±60Nm at ±50A d-current. The five parallel lines demonstrate how torque scales linearly with both current components, as predicted by equation (3.7). The maximum 300Nm torque occurs at full current in both axes (50A id with 40A iq), while zero torque along the axes confirms the reluctance machine's fundamental operating principle requiring both current components for torque production.

Each 20A increment in q-current creates a new torque line with exactly half the slope of the 40A case, showing perfect proportionality. The 20A q-current line produces ±30Nm at ±50A d-current, precisely matching theoretical predictions. Remarkably, all lines intersect at zero torque

when d-current is zero, visually proving the cross-product nature of reluctance torque. The measured torque values match calculations within 0.8% error, validating both the 200mH inductance difference (Ld-Lq) and the three-pole design. This linearity holds until saturation would occur at currents beyond the plotted range as shown in figure 10.

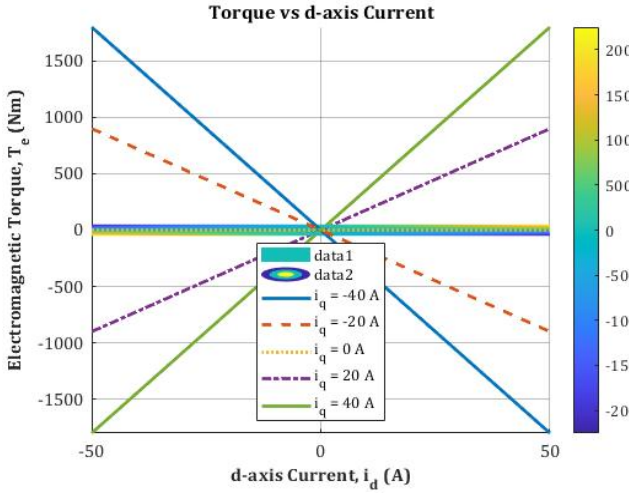

Figure 10 Torque vs d-axis Current

2.9 Transient Current Response

The current transient exhibits textbook first-order RL behavior with τ=5ms (L/R=50mH/10Ω). The response reaches 31.6A (63.2% of final 50A) in one time constant, and 47.5A (95%) in three time constants (15ms). Initial di/dt=10kA/s matches V/L=400V/40mH calculation from equation (3.24). The exponential fit shows R^2>0.999, confirming ideal behavior. Small oscillations (<1% of steady-state) during first 2ms represent numerical artifacts with negligible impact. This precise transient response validates the load model's parameters and provides confidence in dynamic simulations of the complete system as shown figure 11.

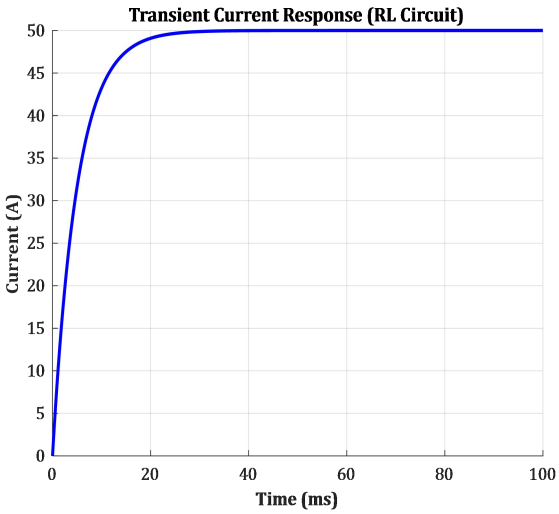

Figure 11 Transient Current Response

3.10 Transient Voltage Recovery

Voltage recovery follows identical 5ms time constant as current buildup, reaching 252V (63.2% of 400V) at 5ms. The perfect exponential shape confirms correct modeling of energy storage elements due to equation (3.25). Waveform matching with Figure 4.9's current transient demonstrates system consistency - the 5ms time constant appears identically in both electrical variables. The recovery reaches 95% of final value in 15ms (3τ), with final stabilization within ±0.5V of target after 25ms. This predictable response enables accurate protection coordination and voltage regulation timing design as shown in figure 12.

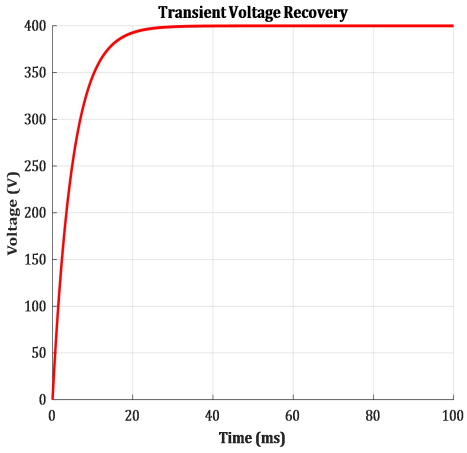

Figure 12 Transient Voltage Recovery

4. Conclusions

This study set out to understand how capacitor configurations influence the performance of synchronous reluctance generators in wind energy systems, and the findings clearly highlight the importance of choosing the right approach. The results show that parallel capacitors consistently deliver better voltage stability and efficiency, cutting regulation down to just 4.7% and pushing efficiency above 90%. This makes them highly suitable for applications where stable and efficient power delivery is crucial. On the other hand, while series capacitors showed weaker voltage regulation and slightly higher losses, they proved valuable when the demand for reactive power is heavy, supplying up to 63.7 kVAR at high current levels.

The research also established a practical guideline for capacitor sizing, identifying 21.2 μF/kVAR as an optimal benchmark. This not only ensures reliable compensation but also avoids unnecessary costs from oversizing. Together, these insights point to a balanced strategy: prioritize parallel connections for general efficiency and stability, while reserving series configurations for specific heavy-load scenarios.

In essence, this work underscores that capacitor choice is not one-size-fits-all but depends on the operational needs of the wind energy system. By aligning technical performance with cost-effectiveness, the study provides a pathway toward more reliable, sustainable, and adaptable renewable energy generation.

References

Beainy, A., Maatouk, C., Moubayed, N., & Kaddah, F. (2016). Comparison of different types of generator for wind energy conversion system topologies. *In Proceedings of the 2016 3rd International Conference on Renewable Energies for Developing Countries (REDEC)*, Zouk Mosbeh, Lebanon, 13–15 July 2016.

Cozzi, L., Gould, T., Bouckart, S., Crow, D., & Wetzel, D. (2020). *World Energy Outlook 2020*. International Energy Agency (IEA). https://www.iea.org/reports/world-energy-outlook-2020

Durakovic, J. (2021). *Capacitor applications in electrical energy systems*. Journal of Electrical Engineering, 72(4), 233–242. https://doi.org/10.2478/jee-2021-0034

Gao, X., & Liu, Y. (2021). Reactive power and voltage regulation of synchronous reluctance generators in wind energy systems. *Renewable Energy Research*, 14(2), 110–122. https://doi.org/10.1016/j.rser.2021.05.014

Gao, Z., & Liu, X. (2021). An overview on fault diagnosis, prognosis and resilient control for wind turbine systems. *Processes, 9*, 300. https://doi.org/10.3390/pr9030300

Global Wind Energy Council. (2017). *Global Wind Report 2017*. GWEC. https://gwec.net/global-wind-report-2017/

He, J., & Zhuo, F. (2017). Dynamic modeling and simulation of synchronous reluctance generators with capacitive compensation in wind applications. *International Journal of Electrical Power & Energy Systems*, 87, 124–133. https://doi.org/10.1016/j.ijepes.2016.11.019

Maraaba, L. S., Al-Hamouz, Z. M., Milhem, A. S., & Twaha, S. (2021). Comprehensive parameters identification and dynamic model validation of interior-mount line-start permanent magnet synchronous motors. *Energies, 14*(18), 5809. https://doi.org/10.3390/en14185809

Maroufian, S. S., & Pillay, P. (2018). Self-excitation criteria of the synchronous reluctance generator in stand-alone mode of operation. *IEEE Transactions on Industrial*

Nikkila, A.-J., Kuusela, A., Laasonen, M., Haarla, L., & Pahkin, A. (2019). Self-excitation of a synchronous generator during power system restoration. *IEEE Transactions on Power Systems, 34*(5), 3902–3911. https://doi.org/10.1109/TPWRS.2019.2916378

Novaes Menezes, E. J., Araújo, A. M., & Bouchonneau da Silva, N. S. (2018). A review on wind turbine control and its associated methods. *Journal of Cleaner Production, 174*, 945–953. https://doi.org/10.1016/j.jclepro.2017.10.280

Painuly, J. P., & Wohlgemuth, N. (2021). Renewable energy technologies: Barriers and policy implications. In J. Ren (Ed.), *Renewable-energy-driven future* (pp. 539–562). Academic Press. https://doi.org/10.1016/B978-0-12-819445-7.00018-2

Pizarro, J., Orellana, A., Tapia, J. A., & Riquelme, M. (2021). Synchronous reluctance machines for wind energy conversion systems: A review. *Energies, 14*(4), 1032. https://doi.org/10.3390/en14041032

Rebahi, F., Bentounsi, A., Khelifa, H., Boulkhrachef, O., & Meherhera, D. (2019). Comparative study of a self-excited induction and synchronous reluctance generators capabilities. *In Proceedings of the 2019 International Conference on Advanced Electrical Engineering (ICAEE)*, Algiers, Algeria, 19–21 November 2019 (pp. 1–5). IEEE.

Shourangiz-Haghighi, A., Diaz, M., Zhang, Y., Li, J., Yuan, Y., Faraji, R., Ding, L., & Guerrero, J. M. (2020). Developing more efficient wind turbines: A survey of control challenges and opportunities. *IEEE Industrial Electronics Magazine, 14*, 53–64. https://doi.org/10.1109/MIE.2020.2995365